Vol. 22 • No. 10 • March 12 • 2010

D10488

www.advmat.de

ADVANCED MATERIALS

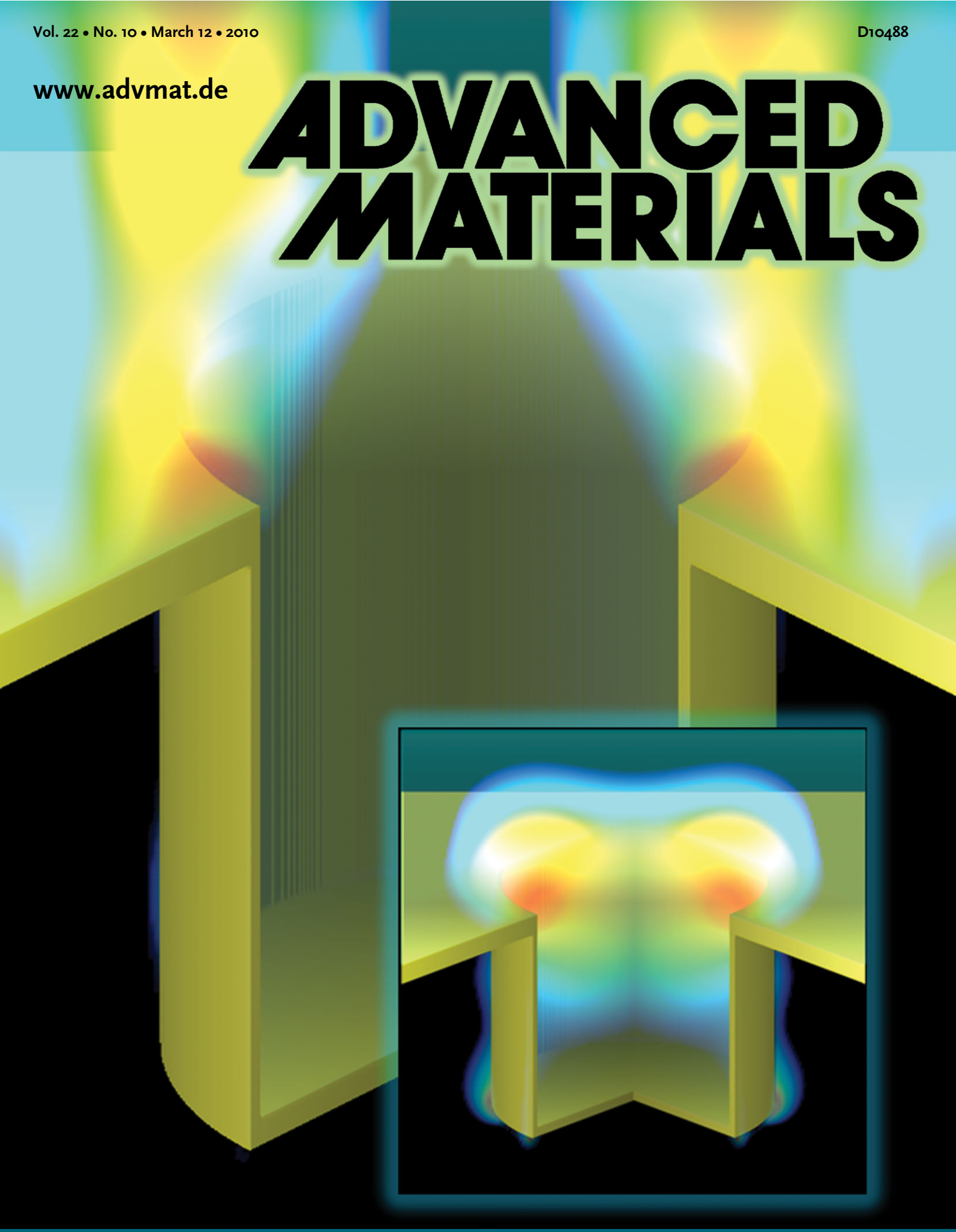

WILEY-VCH

Nanostructured Plasmonic Materials

ADVANCED MATERIALS
www.advmat.de

www.MaterialsViews.com

Functional Nanostructured Plasmonic Materials

By *Jimin Yao, An-Phong Le, Stephen K. Gray, Jeffrey S. Moore, John A. Rogers,* and *Ralph G. Nuzzo**

Plasmonic crystals fabricated with precisely controlled arrays of subwavelength metal nanostructures provide a promising platform for sensing and imaging of surface binding events with micrometer spatial resolution over large areas. Soft nanoimprint lithography provides a robust, cost-effective method for producing highly uniform plasmonic crystals of this type with predictable optical properties. The tunable multimode plasmonic resonances of these crystals and their ability for integration into lab-on-a-chip microfluidic systems can both be harnessed to achieve exceptionally high analytical sensitivities down to submonolayer levels using even a common optical microscope, circumventing numerous technical limitations of more conventional surface plasmon resonance techniques. In this article, we highlight some recent advances in this field with an emphasis on the fabrication and characterization of these integrated devices and their demonstrated applications.

1. Introduction

Surface plasmons result from incident electromagnetic radiation exciting coherent oscillations of conduction electrons near a metal-dielectric interface.[1–3] These oscillations result in an evanescent electric field that extends from the metal surface into the dielectric over a length scale on the order of hundreds of nanometers.[4] This field allows surface plasmons to respond to changes in the local refractive index with high sensitivity, which in turn provides a capability for label-free forms of analytical detection. For example, surface plasmon resonance (SPR) measurements are now commonly used to detect and quantify chemical and biological analytes without the need for fluorescent or radioactive labels.[5,6] SPR measurements can be carried out in both single-mode spectroscopic and multiplexed imaging protocols.[7–9]

The standard SPR method noted above makes use of the properties of surface plasmons in the form of surface plasmon polaritons (SPPs). SPPs are evanescent surface waves on metal films which propagate along the metal-dielectric interface.[10] SPP propagation lengths are typically tens to hundreds of micrometers along the metal-dielectric interface.[11,12] Techniques employing these propagating plasmons most commonly use a prism to couple light into the metal film (typically gold) in the Kretschmann configuration[13–15], although gratings can also couple light into SPPs.[16,17] The cumbersome nature of such optics, however, makes it difficult to integrate these techniques into portable, low-cost devices and high-throughput systems.[18] These limitations can be overcome through the use of metallic nanostructures such as metal nanoparticles, line gratings, and hole arrays in metal films, structures that each provide efficient optical coupling mechanisms through which to excite plasmons.[4,17,19–21] These systems also give rise to localized surface plasmon resonances (LSPRs) which can be tuned by carefully controlling the shape, size, and spacing of the nanostructures.[22–26] In contrast to propagating SPPs, LSPRs are confined around the objects being excited and can have higher intensities. LSPRs can thus be exploited to make measurements with higher spatial resolution than would be possible using propagating SPPs.[4,21,27–29]

Surface plasmon excitations are also linked to the enhancement factor observed in surface-enhanced Raman spectroscopy (SERS).[24,30–34] The roughened metal films classically used as SERS substrates[35–37] couple incident light to surface plasmons with enhancement factors of 10^{10}–10^{12} commonly obtained in single molecule SERS studies.[30,38–43] The full utility of SERS has not yet been realized with these substrates, however, because they suffer from poor reproducibility.[30] Recent work in this field has explored the use of more precisely defined metal nanoparticles[44] and nanowires[45], as well as nanoscale holes[46,47] and voids[48] in metal films as SERS substrates. These structures may provide more reliable performance while still leading to reasonably large

[*] Prof. R. G. Nuzzo, J. Yao, A.-P. Le
Department of Chemistry, University of Illinois
600 South Mathews Avenue, Urbana, IL 61801 (USA)
E-mail: r-nuzzo@illinois.edu
Dr. S. K. Gray
Center for Nanoscale Materials
Argonne National Laboratory, Argonne, Illinois 60439 (USA)
Prof. J. S. Moore
Department of Chemistry, University of Illinois
600 South Mathews Avenue, Urbana, IL 61801 (USA)
Prof. J. A. Rogers
Department of Materials Science and Engineering, Frederick Seitz Materials Research Laboratory, University of Illinois
104 S. Goodwin Ave., MC-230 Urbana, IL 61801 (USA)

DOI: 10.1002/adma.200904097

SERS enhancement factors. Ideally, these substrates would be fabricated using techniques that generate nanostructured patterns over large substrate areas with high fidelity and high control at low cost. The design rules for these optics, however, can be quite demanding and for this reason difficult to realize in practice except via the application of demanding forms of lithography and thin-film processing.

Electron beam lithography and focused ion beam lithography, for example, have been used to fabricate arrays of gold particles,[49,50] circular slits,[51] nanoholes,[52,53] and v-shaped grooves in metal films.[54] These fabrication methods provide high precision and control over the dimensions of the nanostructures. It is difficult, however, to generate patterns over large areas using these methods, and they are limited to serial sample fabrication.

An alternative method, nanosphere lithography,[55,56] uses a hexagonally close-packed monolayer of spheres on a surface as a deposition or etch mask for the generation of metal nanoparticles in the interstices between spheres[57] or as a substrate for the creation of metal-film-over-nanosphere structures.[58] Colloidal lithography is a closely related technique where spheres are adsorbed onto a surface, but the spheres are usually more randomly distributed than in nanosphere lithography.[59,60] Defect-free nanostructured regions with areas approximately 10–100 μm^2 can be routinely formed using nanosphere lithography.[57]

More recent reports document the fabrication of large area plasmonic nanostructures using soft interference lithography.[61–63] In this method, an elastomeric master is replicated from a master generated by interference lithography and is used as a phase mask for phase-shifting photolithography on a silicon wafer. A metal film is evaporated onto the resulting photoresist structure, and lift-off of the photoresist leaves a continuous metal film with an array of holes or voids. Additional etching and metal evaporation steps generate free-standing metal films with precisely controlled hole structures which can then be transferred onto a support material.[64,65] Using this method, centimeter-scale areas of high quality nanostructures, ones well modeled within finite-difference time-domain calculations, can be realized.[61,66] Although common processing techniques are exploited here (interference lithography, wet chemical etching, metal evaporation, lift-off), the multiple steps required add complexity to the fabrication processes. More importantly, there remains a need to generalize the process, while retaining the capacity for low cost, in ways that can reach more challenging design rules and accommodate large area format or topologically complex substrates.

Soft nanoimprint lithography has shown promise as a method to satisfy such needs – it is able to pattern large area arrays (greater than 10 mm^2) of nanostructures with a resolution of less than 100 nm at relatively low cost.[4,67–69] We have used soft nanoimprint lithography to fabricate large and highly reproducible arrays of cylindrical nanowells for use as SPR sensors and SERS substrates. These easily produced nanoimprinted structures have also demonstrated submonolayer sensitivities for detecting binding events with limits of detection rivaling those of more conventional SPR devices. The micrometer-level lateral resolution over millimeter length scales enables highly sensitive and fully quantitative forms of imaging using both SPR and SERS over areas larger than those accessible through other device geometries and fabrication methods.

Ralph G. Nuzzo is the G. L. Clark Professor of Chemistry and a Professor of Materials Science and Engineering at the University of Illinois at Urbana-Champaign. He received his B.S. degree in Chemistry from Rutgers College in 1976 and his Ph.D. degree in Organic Chemistry from the Massachusetts Institute of Technology in 1980. He is a fellow of the American Academy of Arts and Sciences and currently serves as a Senior Editor of Langmuir.

2. Nanostructured Plasmonic Crystals

There are several features of plasmonic crystals such as those shown in Figure 1 that motivate their consideration over nanoparticles for applications in sensing. First and foremost, the precisely controlled details of their structure enable reliable

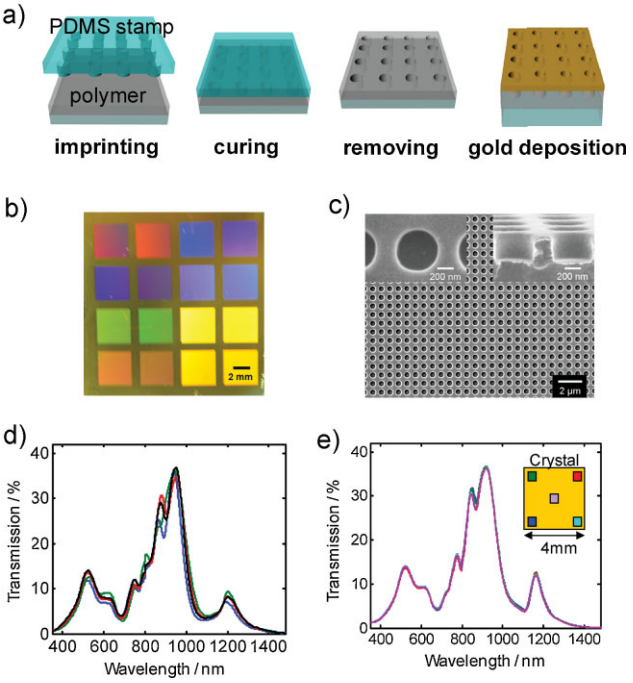

Figure 1. a) Schematic illustration of soft nanoimprint lithography protocol. b) Optical image of an embossed plasmonic crystal. Hole depth is ~400 nm, hole diameters vary from ~0.24 to ~1.06 μm, and hole spacings vary from ~0.50 to ~1.74 μm. c) SEM image of cylindrical hole array patterned by soft nanoimprint lithography with insets of an individual hole and a cross section view. Figure 1a–c were adapted and reproduced with permission from [29]. d) Overlay of transmission spectra for four separate plasmonic crystal samples showing similar optical response between samples. e) Overlay of transmission spectra taken from five areas within a single array on a plasmonic crystal showing nearly identical response across entire array area. The plasmonic crystal used for (d) and (e) had a hole depth of ~350 nm, a hole diameter of ~456 nm, and a hole spacing of ~748 nm.

simulations of the electromagnetic fields and optical properties by rigorous computational electrodynamics methods such as the finite-difference time-domain (FDTD) method.[26,66,70–72] Their uniformity allows for sensing and imaging of surface binding interactions with high analytical sensitivity down to even submonolayer levels.[4,28,29] The spectroscopic responses of these devices can be shifted across near-IR and visible wavelengths by adjusting feature sizes, spacings, and depths or by more simply adjusting the thin metal film distribution without altering the design rules of the device (the latter avoiding the fabrication of a new lithographic master).[4,29] The achievable sensitivity of plasmonic crystals at visible wavelengths is quite substantial, sufficient to differentiate molecular binding in a patterned self-assembled monolayer even for cases where domains of the adsorbates have a mass difference of only two carbon atoms.[29] The platform also provides a facile means for effecting chemically-coupled forms of sensing, enabling in turn other interesting applications including pH sensing[73] and SERS mapping.[34]

This section describes representative classes of plasmonic crystals developed in our work and the means employed to fabricate them. One is a quasi 3D plasmonic crystal with high sensitivity at near IR wavelengths, and the other one is a full 3D plasmonic crystal with high sensitivity in the visible region. We consider in this report the progress made to provide theoretical characterizations of their properties along with examples of applications exploiting their unique capacities.

2.1. Plasmonic Crystal Fabrication and General Characterization

A simple, robust, and low-cost soft nanoimprint lithography protocol (illustrated in Figure 1a) is used to fabricate sub-wavelength hole arrays over large areas.[4,29,34,68,74] To do so, a molded polydimethylsiloxane (PDMS) stamp[75–78] with square arrays of cylindrical post relief features is used to emboss a thin layer of a curable material, most commonly a photocurable polyurethane cast onto a glass slide. The sample is then exposed to ultraviolet light to cure the polyurethane layer. Careful removal of the PDMS stamp leaves a relief structure complementary to the pattern on the PDMS stamp imprinted in the polyurethane layer surface. This nanoimprint method can be adapted to broadly accommodate materials of diverse form and thus is not limited to using a PDMS patterning tool to emboss polyurethane layers. Other materials with low surface energy and good chemical resistance like perfluoropolyether [79–82] can also be used to mold other materials (e.g., an SU8 photoresist precursor) to form embossed substrates for plasmonic nanostructures with high replication fidelity.[74,79] In our work, we typically employ a non-metallic adhesion layer that does not quench the plasmonic response to provide devices that are robust to the environments found in analytical applications.[83–85] Finally, a thin gold film is deposited on the patterned substrate either by electron beam evaporation to form a quasi 3D plasmonic crystal or by sputter deposition to form what we term a full 3D plasmonic crystal. The differences between ''quasi'' and ''full'' 3D plasmonic crystals will be made more clear below. This reliable and robust nanoimprint method can generate nanostructures over large areas with high spatial uniformity as the discussions below demonstrate.

A typical optical photograph of an embossed plasmonic crystal is shown in Figure 1b. There are sixteen 4 mm × 4 mm square arrays of nanowells with different hole diameters and periodicities on each plasmonic crystal. The uniform diffraction colors produced by these structures further demonstrate the exceptional quality of the features generated by the soft nanoimprint lithography process, one possessing resolution that can reach to molecular levels.[76] Figure 1c shows scanning electron microscopy (SEM) images from one square of a full 3D plasmonic crystal array. The specific patterned area shown consists of a square array of cylindrical depressions with diameters of 456 nm, a periodicity of 748 nm, and depths of 350 nm. The high resolution SEM insets demonstrate the formation of a continuous gold layer on the embossed polyurethane nanostructures. Transmission electron microscopy measurements of the gold layer thicknesses show differences between the layers on the top surface, sidewall, and well bottom. These thicknesses are critical for tuning the multiple plasmonic resonance features of the full 3D plasmonic crystal. In contrast, the gold coverage of the quasi 3D plasmonic crystal is discontinuous, consisting of a continuous top layer of gold with nanoholes and separated gold disks at the bottom of the embossed depressions. These differences lead to pronounced and distinctive qualities of the optics for measurements made either at visible or near IR wavelengths.

The use of PDMS elastomer in nanoimprint lithography enables the fabrication of many polymer nanostructures from a single PDMS stamp with high replication fidelity. Additionally, PDMS stamps can be accurately replicated many times from a single photolithographic master. This property is illustrated by the data in Figure 1d, which displays normal incidence transmission spectra of four different full 3D plasmonic crystals replicated from a single PDMS stamp, all of which show very similar spectroscopic responses. Spectra taken from different areas within a single square of a full 3D plasmonic crystal, shown in Figure 1e, again show very similar responses across the entire millimeter scale area.

2.2. Computational Studies of Plasmonic Features and Bulk Sensitivity Calibration

The multiple plasmonic resonances provided by a typical plasmonic crystal device can be predicted through rigorous computational electrodynamics calculations.[70,71] Full 3D FDTD calculations (Fig. 2) with appropriate periodic boundary conditions were carried out to model the normal incidence transmission spectra and electromagnetic field distributions associated with selected resonances for the systems shown in Figure 1. The multiple features in the transmission spectra of these plasmonic crystals can be associated with LSPRs[24,86,87], Bloch wave SPPs (BW-SPPs) [70], and Wood anomalies[4,19,70], or combinations of these features[66], and the coupling of directly transmitted light through the gold film. While the LSPRs can be generated in the random arrays of holes and particles, BW-SPPs and Wood anomalies are created by the grating defined by the spatially

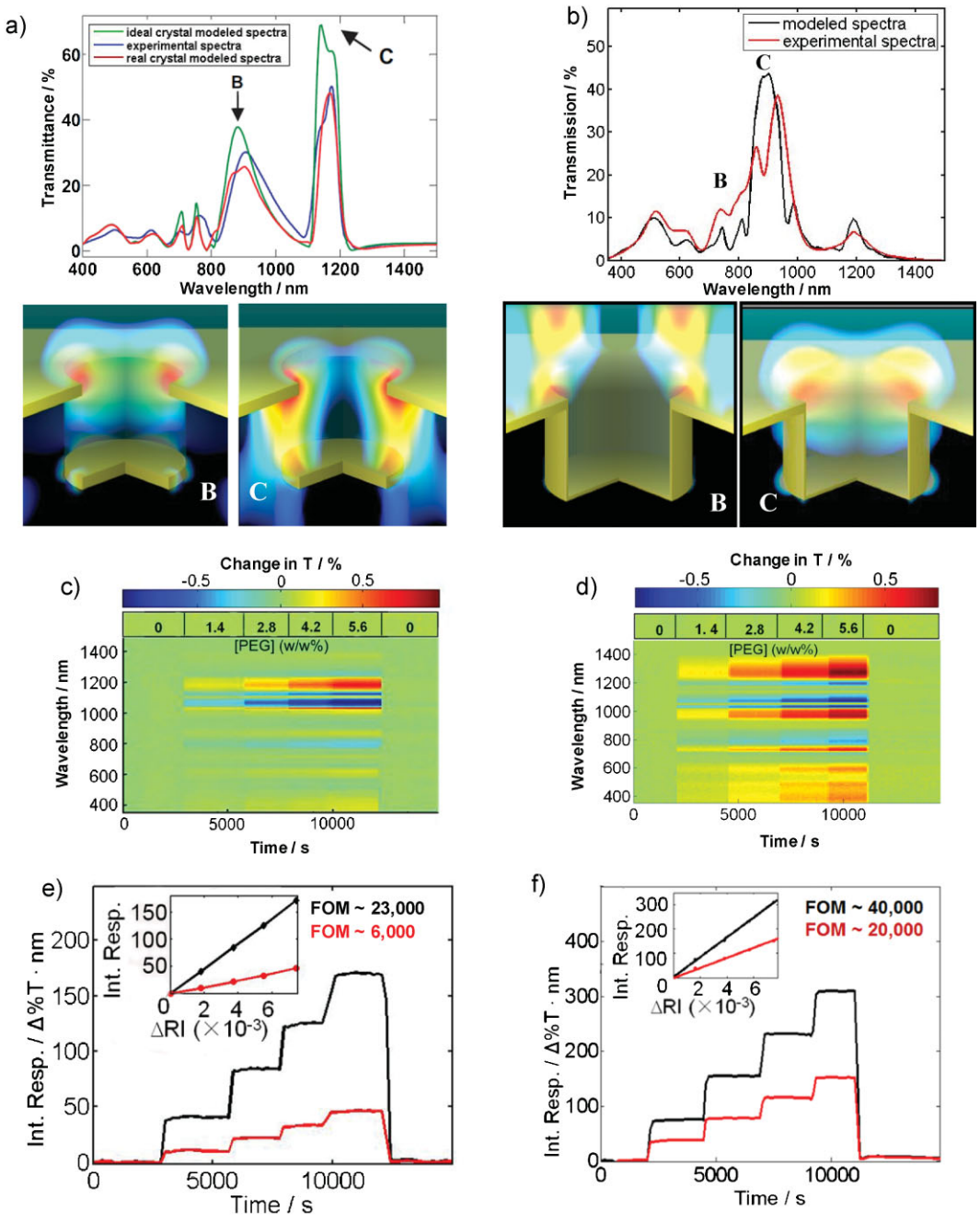

Figure 2. a) Experimental transmission spectrum (blue) for quasi-3D plasmonic crystal (~420 nm hole diameter, ~350 nm hole depth, ~720 nm hole spacing) and electrodynamic modeling transmission spectra with idealized gold distribution (green) or with isolated gold grains near edge of bottom gold disc (red); calculated electric field plots (bottom images) corresponding to wavelengths for peaks marked B and C in the plot above. Figures were adapted and reproduced with permission from [4]. Copyright 2006, National Academy of Sciences. b) Experimental transmission spectrum (black) for full-3D plasmonic crystal (~456 nm hole diameter, ~350 nm hole depth, ~748 nm hole spacing) and electrodynamic modeling transmission spectrum (red); calculated electric field plots (bottom images) corresponding to peaks marked B and C in the plot above. Figures were adapted and reproduced with permission from [29]. c) Spectral difference map for quasi-3D plasmonic crystal bulk refractive index sensitivity measurement. d) Spectral difference map for full-3D plasmonic crystal bulk refractive index sensitivity measurement. e) Integrated response of quasi-3D plasmonic crystal with inset showing linear change in average integrated response with refractive index change f) Integrated response of full-3D plasmonic crystal with inset showing linear change in average integrated response with refractive index change. Red trace in (e) and (f) corresponds to integration from 355–1000 nm, black trace in (e) and (f) corresponds to integration from 355–1500 nm.

coherent periodicity of ordered arrays. BW-SPPs may be viewed as standing waves formed from superpositions of counterpropagating SPPs. Wood anomalies require just a grating structure and may be viewed as diffractive, not plasmonic, features. The wavelengths corresponding to Wood anomaly excitations are often close to those of BW-SPPs.

All the features noted are sensitive to the minute structural details and dielectric properties of the surrounding environment.[4,29] Careful consideration of the Au film distribution on the nanowell array is critical to achieve good agreement between experiment and theory for both the full 3D and quasi 3D plasmonic crystal systems.[4,29] The different spectroscopic responses of these plasmonic crystals, tuned by the gold film distributions, revealed different dominant plasmonic modes. The largest feature in the quasi 3D transmission spectrum labeled C (Fig. 2a) can be assigned to BW-SPP and Wood anomaly excitations with a strong electric field intensity near the gold disk/polymer interface and strong coupling between the upper and lower levels of the quasi 3D crystal. In contrast, the second large feature labeled B in the quasi 3D transmission spectrum (Fig. 2a) can be identified with a LSPR excitation isolated at the edge of the nanowell near the air/gold interface. These strong plasmonic resonances are responsible for the high sensitivity of the quasi 3D crystal in the near IR region to refractive index changes observed in angle-dependent transmission experiments,[68] enabling one- and two-dimensional imaging of surface bindings at near-IR wavelengths and quantitative multispectral biosensing capabilities.[4,28] On the other hand, the largest plasmonic feature labeled C in the full 3D plasmonic crystal transmission spectrum (Fig. 2b) is the result of LSPR excitations with strong electric field intensities close to the nanowell sidewalls and spanning across the nanowell opening. The spectral feature labeled B in the transmission spectrum of the full 3D plasmonic crystal is due primarily to a combination of effects from BW-SPPs and LSPRs. These plasmonic resonances are blue-shifted from the near IR to visible wavelengths, guided by the confinement effects and complex interactions of the various diffractive and plasmonic modes supported by the design rule of the full 3D plasmonic crystal. The important point to note here, however, is that the pronounced sensitivity of the full 3D plasmonic crystal in the visible region allows molecular imaging with submonolayer resolution using a common optical microscope and low-cost charge-coupled device (CCD) camera.

The sensitivity of plasmonic systems to the change of bulk refractive index is usually determined by measuring the change of a single resonance feature with changes in the surrounding refractive index.[88,89] This single resonance analysis method cannot fully capture the sensitivity of a multiple resonance plasmonic system. We therefore have developed a full multispectral analysis method to calibrate the sensitivity of our systems by using all of the spectral feature changes in an accessible wavelength range. This multispectral analysis not only distinguishes the sensitivity of our system from that of literature reported 2D grating or random array systems[18,86,88–93] but also provides a means to improve the signal-to-noise ratio of our measurements many fold.[4] In our bulk sensitivity measurement, for example, normal incidence transmission spectra were collected over time as solutions of increasing refractive index were flowed over the surface of the plasmonic crystal. The collected spectra were then referenced to the initial spectrum to generate the spectral difference map shown in Figure 2c for the quasi 3D plasmonic crystal and in Figure 2d for the full 3D plasmonic crystal. Both the transmission spectral intensity changes and the peak position shifts over the measured wavelengths are collected by the spectral difference map. The plasmonic feature changes are wavelength dependent and can be both positive and negative at different wavelengths as a function of refractive index change. In order to fully capture these changes, the absolute magnitudes of spectral differences are integrated to provide the total spectroscopic response of the sensor and plotted as a function of time as shown in Figure 2e and 2f for the quasi 3D and full 3D systems, respectively. The linear changes of the integrated response in our systems as a function of refractive index unit (RIU) change in the surrounding fluid yields a figure of merit for our systems with units of Δ%T nm RIU^{-1}. The quasi 3D system exhibits the highest sensitivity at wavelengths between 1000–1250 nm, but the sensitivity is more than $3\times$ lower than that of the full 3D system in the wavelength range of 350–1000 nm. The linearity of the spectral response of our systems suggests an ideal platform for quantitative multispectral biosensing and imaging.

Recently we have shown, based on FDTD calculations, that it is possible to further optimize the bulk refractive index sensing capabilities of plasmonic crystals.[26] In this work, different system parameters (metal film thicknesses, hole diameters and relief depths, etc.) were varied, and an order of magnitude improvement in the figure of merit was predicted.

2.3. Optical Imaging Demonstrations

The excellent spatial uniformity seen over large image areas for these optical systems provides a solid foundation for fully quantitative imaging applications. The high sensitivity over near IR wavelengths of the quasi 3D plasmonic crystal enables near IR imaging, whereas the enhanced sensitivity in the visible region of the full 3D plasmonic crystal provides direct imaging capabilities with white light.

In demonstration experiments, nonspecifically adsorbed fibrinogen line arrays were patterned on top of quasi 3D plasmonic crystals and imaged in 1D and 2D modes using monochromatic illumination and white light.[4,28] The top image in Figure 3a is a white light image of these fibrinogen arrays, and the bottom image was acquired using monochromatic light at 1090 nm; both images were captured using an IR camera. The fibrinogen lines appear darker than the uncoated regions in the white light image because the total decrease in transmission is larger than the total increase in transmission across the wavelength range of the camera. In contrast, the fibrinogen patterned regions are brighter than the uncoated regions imaged at 1090 nm because of the increased transmission at this wavelength due to the surface binding.[28] The spatial resolution of the resolved image using quasi 3D plasmonic crystals is on the order of tens of micrometers with a submonolayer detection limit.[28] More importantly, the optical response of this system in imaging mode can be converted to an effective surface coating thickness by applying the appropriate calibration constants

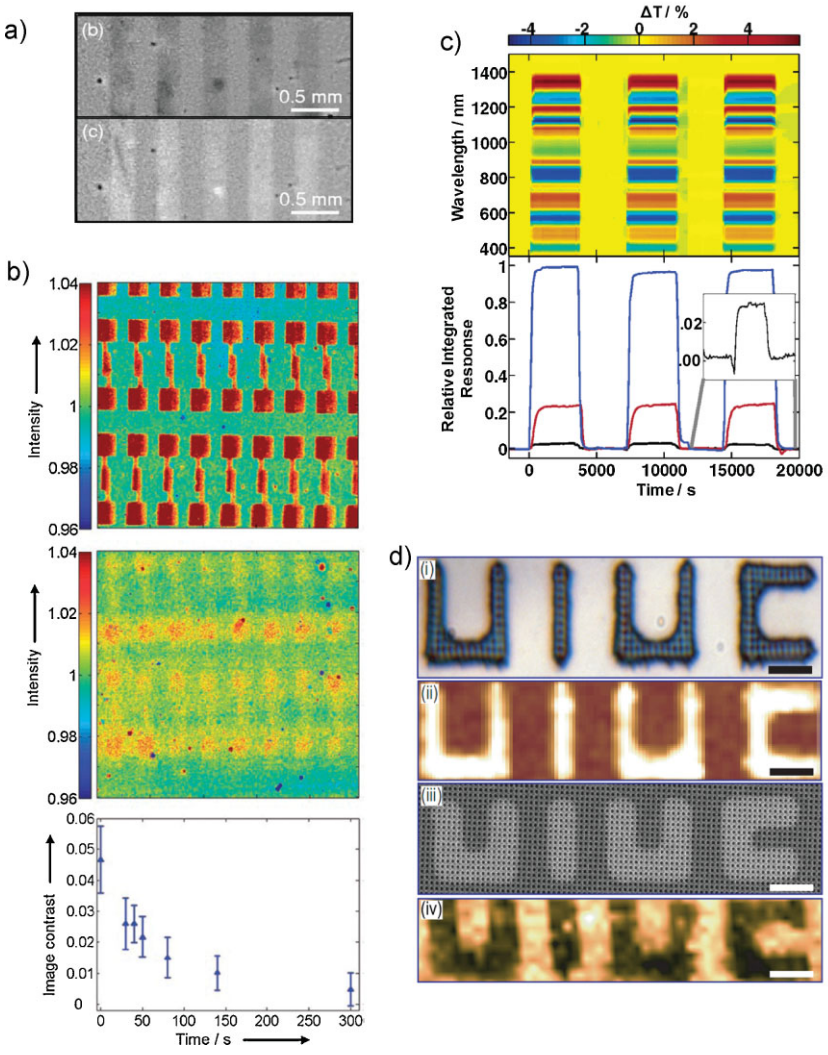

Figure 3. a) Optical images of fibrinogen lines illuminated with white light (top) and light at 1090 nm (bottom) patterned on quasi-3D plasmonic crystal. Figures were adapted and reproduced with permission from [28]. Copyright 2007, American Institute of Physics. b) Optical images of 1-octadecanethiol patterned onto full-3D plasmonic crystal before backfilling with 1-hexadecanethiol (top) and after backfilling (middle) and calculated image contrast over time during backfilling (bottom). Figures were adapted and reproduced with permission from [29]. c) Spectral difference map for pH changes in hydrogel-modified quasi-3D plasmonic crystal (top) and relative integrated responses for pH changes of 7.86 to 1.44 (blue), 6.42 to 5.13 (red), and 5.76 to 5.66 (black) (bottom), inset is a vertically magnified view of the black curve. Figures were adapted and reproduced with permission from [73]. Copyright 2007, American Chemical Society. d) Optical image (i) and SERS mapping (ii) of benzenethiol monolayer on quasi-3D nanohole array imprinted in previously photodefined SU-8; SEM image (iii) and SERS mapping (iv) of 1-octadecanethiol "UIUC" microcontact printed onto quasi-3D nanohole array and backfilled with benzenethiol. Figures were adapted and reproduced with permission from [34]. Scale bars are 5 μm. Copyright 2009, American Institute of Physics.

obtained from bulk sensitivity measurements in a simple formalism.[4,28,94]

The increased sensitivity at visible wavelengths of the full 3D plasmonic crystal makes possible the imaging of molecular binding over large areas using a common optical microscope with an inexpensive silicon CCD. As a demonstration, we imaged a pattern of two different alkanethiols on the full 3D plasmonic crystal with white light. The transmitted-light image of a microcontact printed[95] 1-octadecanethiol (ODT) self-assembled monolayer pattern[96–100] with a thickness of ~ 2nm is displayed in the top image of Figure 3b. The imaging contrast clearly differentiates ODT patterned regions from uncoated regions with high signal-to-noise level due to the refractive index difference between these areas. The spatial resolution of the plasmonic imaging using the full 3D plasmonic crystal can reach ~3 micrometers as judged from a quantitative lineshape analysis.[29] To highlight the submonolayer detection resolution, we soaked the ODT printed full 3D plasmonic crystal in a 1-hexadecanethiol (HDT) solution and monitored the imaging contrast decrease as a function of time. The middle image in Figure 3b illustrates the transmitted-light image of the ODT patterned sample after backfilling with HDT for 300 s. The patterned ODT regions are less distinct at the end point of the backfilling experiment because of the reduced refractive index difference between the ODT regions and the HDT filled areas. The plot of the image contrast decrease as a function of backfilling time (Fig. 3b, bottom panel) resembles an inverted first-order Langmuir adsorption isotherm.[29] The image contrast after the backfilling process, which is about 10% of the initial value, correlates well with the two-carbon atom difference in the ODT and HDT molecules. These results demonstrate the exceptional analytical sensitivity of the full 3D plasmonic crystal motif in quantitative white light imaging.

2.4. Optical Imaging of Chemical Forces

SPR response is not limited to detecting significant refractive index changes on or near the plasmonic crystal surface. Chemical forces associated with essentially no refractive index change can also be transduced to SPR responses by combining the plasmonic system with other analytically relevant parameters provided by chemometric actuators, such as pH responsive acrylic acid modified hydrogels.[101–103] We have previously reported a hydrogel-modified plasmonic crystal system for amplifying the analytical power of the plasmonic system by coupling the SPR resonance features with hydrogel swelling dynamics.[73] A pH-responsive hydrogel film with a thickness of ~500 nm was covalently bound to the gold surface of a quasi 3D plasmonic crystal. This cross-linked polymer network swells in basic solutions and contracts in acidic solutions.[73,104] The

normalized spectral difference map shown in the top panel of Figure 3c illustrates the reversible plasmonic responses of a pH-responsive hydrogel-modified plasmonic crystal corresponding to the cycling between two limiting pH conditions. The plasmonic responses decrease with a decrease in the pH change centered around the pKa of the hydrogel. The bottom panel of Figure 3c shows the relative integrated response for the change in transmission when the pH of the solution was changed from 7.86 to 1.44 (blue), 6.42 to 5.13 (red), and 5.76 to 5.66 (black). The changes in this hydrogel are clearly reversible as the pH is adjusted back and forth, and a pH change of 0.10 is clearly distinguishable from the background as shown in the inset. The plasmonic responses of this device are much larger than those of an unmodified plasmonic crystal. Measurements on a hydrogel without acrylic acid showed much lower spectral response to pH changes across the entire wavelength range. The addition of acrylic acid enhanced the swelling of the hydrogel by enhancing the change in osmotic pressure within the hydrogel relative to the covalent bonds holding the polymer network intact.[101,102]

Although surface plasmons are able to probe the refractive index of the immediate surrounding medium, the hydrogel films here are thicker than the penetration depth of the evanescent electric fields supported by these plasmonic crystals.[4] The observed optical changes are thus an indirect measure of the change in volume and a way to measure the mechanical forces exerted as the hydrogel changes volume. Although a proton gradient was used to swell and collapse the hydrogel in this work, other analytes of interest in principle can be similarly measured by adding an appropriate recognition system to the hydrogel network.

2.5. SERS Imaging

Plasmonic nanohole arrays are effective substrates for SERS spectroscopy and imaging.[34] In an exemplary demonstration, quasi 3D plasmonic crystals were made using the same fabrication procedures described earlier for the production of arrays for SPR systems. After metalizing the molded polymer with gold, the arrays were soaked in ethanolic solutions of benzenethiol to form a monolayer on the array surface. SERS spectra of benzenethiol were collected using a Raman microscope and an excitation wavelength of 785 nm. Signal enhancement factors of $\sim 10^5$ were observed using non-optimized substrates (using the SERS signal at $\sim 1073\ cm^{-1}$) based on a square array of 514 nm holes, 360 nm deep, and with a periodicity of 760 nm. A maximum SERS enhancement is expected when the wavelength of the LSPR feature is equal to the average of the excitation wavelength and the wavelength of the Raman signal.[44] In these experiments, this corresponds to a wavelength of ~821 nm. In fact, the spectral transmission of the plasmonic crystal without benzenethiol at 821 nm correlates well with the measured SERS enhancement factor – the highest enhancement was measured for the nanohole array that had the highest transmission at 821 nm. To a first approximation, the SERS enhancement at a given excitation wavelength can be inferred from electrodynamics calculations, such as FDTD calculations, as the square of the calculated near field intensity enhancement relative to the incident intensity. Therefore, our ability to model the near fields and optical transmission of nanohole array structures may provide an opportunity to design and optimize a structure in silico to maximize the SERS enhancement.

The high uniformity of these nanohole arrays over large areas makes them valuable for SERS-based imaging. The top two images in Figure 3d are of a nanohole array patterned onto previously photodefined SU8. The nanohole array is only present within the letters ''UIUC'' as seen in the optical micrograph (image i). Image ii is a map of the Raman intensity at $1073\ cm^{-1}$ of the same nanohole array after metallization and soaking in benzenethiol. The Raman intensity is clearly higher in the areas where the nanohole array is present. In the bottom two images of Figure 3d, a monolayer of ODT was microcontact printed onto a uniform nanohole array. The rest of the array was backfilled with benzenethiol, and image iii is a SEM image of the inked pattern. Image iv shows the Raman intensity map at $1073\ cm^{-1}$ (where benzenethiol is known to have a response but ODT does not); the image clearly differentiates the two regions. These results show the promise of easily fabricated, highly uniform nanostructures for use as high performance SERS substrates with reproducible responses over large areas.

3. Prospects

The nanoimprinted plasmonic devices described here have combined the exceptional performance of surface plasmon active substrates with rapid and consistent manufacturing techniques and inexpensive materials. These devices provide high analytical sensitivity over tunable wavelength ranges as well as versatile modes of operation. Multiplexed analyses are clearly possible with high spatial and spectral resolution. The integration of portable plasmonic devices with lab-on-a-chip microfluidic systems, combined with the customizable optical properties provided by rigid theoretical simulations, open a promising route to achieve real time label-free detection with submonolayer resolution. Our future work will address important applications that include real time SPR imaging of biochemical systems, providing new forms of dynamic information. For example, our preliminary data suggests that SPR imaging of living cells using a common optical microscope could enable the observation of cell growth behavior and cellular responses to external stimuli, providing valuable new information for understanding cell biology. Miniaturization of the SPR device also brings the possibility of convenient local probe detection and ultra-tracing chemical sensing. Theoretical guidance for optimizing both device form factors and their optical/spectroscopic performance will be of particular importance. Therefore, the development of more accurate and efficient theoretical approaches to simulate and to optimize these systems is a key future direction. The ability to fabricate function by design in this way will constitute a major advance against a long standing, grand challenge in chemical sensing.

Acknowledgements

The authors acknowledge the support of the U.S. Department of Energy, Materials Science Division under award number DE-FG02-07ER46471,

through the Frederick Seitz Materials Research Laboratory (FSMRL) at the University of Illinois. The authors gratefully acknowledge use of the FSMRL Central Facilities, including the Center for Microanalysis of Materials. Use of the Center for Nanoscale Materials was supported by the U. S. Department of Energy, Office of Science, Office of Basic Energy Sciences, under contract number DE-AC02-06CH11357.

Received: November 30, 2009
Published online: January 21, 2010

[1] W. Knoll, *Annu. Rev. Phys. Chem.* **1998**, *49*, 569.
[2] E. Ozbay, *Science* **2006**, *311*, 189.
[3] H. Raether, *Surface plasmons on smooth and rough surfaces and on gratings*, Springer Verlag, Berlin/Heidelberg/New York **1988**.
[4] M. E. Stewart, N. H. Mack, V. Malyarchuk, J. A. N. T. Soares, T.-W. Lee, S. K. Gray, R. G. Nuzzo, J. A. Rogers, *Proc. Natl. Acad. Sci. U. S. A.* **2006**, *103*, 17143.
[5] L.-K. Chau, Y.-F. Lin, S.-F. Cheng, T.-J. Lin, *Sens. Actuators B* **2006**, *113*, 100.
[6] J. Zhao, X. Zhang, C. R. Yonzon, A. J. Haes, R. P. Van Duyne, *Nanomedicine* **2006**, *1*, 219.
[7] H. J. Lee, D. Nedelkov, R. M. Corn, *Anal. Chem.* **2006**, *78*, 6504.
[8] Y. Li, H. J. Lee, R. M. Corn, *Anal. Chem.* **2007**, *79*, 1082.
[9] B. K. Singh, A. C. Hillier, *Anal. Chem.* **2007**, *79*, 5124.
[10] J. Homola, *Chem. Rev.* **2008**, *108*, 462.
[11] B. P. Nelson, A. G. Frutos, J. M. Brockman, R. M. Corn, *Anal. Chem.* **1999**, *71*, 3928.
[12] A. W. Wark, H. J. Lee, R. M. Corn, *Anal. Chem.* **2005**, *77*, 3904.
[13] E. Kretschmann, H. Raether, *Z. Naturforsch. A* **1968**, *23*, 2135.
[14] A. Otto, *Z. Phys.* **1968**, *216*, 398.
[15] J. Homola, *Anal. Bioanal. Chem.* **2003**, *377*, 528.
[16] W. L. Barnes, A. Dereux, T. W. Ebbesen, *Nature* **2003**, *424*, 824.
[17] W. L. Barnes, W. A. Murray, J. Dintinger, E. Devaux, T. W. Ebbesen, *Phys. Rev. Lett.* **2004**, *92*, 107401/1.
[18] N. Nath, A. Chilkoti, *Anal. Chem.* **2002**, *74*, 504.
[19] T. W. Ebbesen, H. J. Lezec, H. F. Ghaemi, T. Thio, P. A. Wolff, *Nature* **1998**, *391*, 667.
[20] L. J. Sherry, S.-H. Chang, G. C. Schatz, R. P. Van Duyne, B. J. Wiley, X. Younan, *Nano Lett.* **2005**, *5*, 2034.
[21] C. R. Yonzon, E. Jeoung, S. Zou, G. C. Schatz, M. Mrksich, R. P. Van Duyne, *J. Am. Chem. Soc.* **2004**, *126*, 12669.
[22] A. J. Haes, R. P. V. Duyne, *Expert Rev. Mol. Diagn.* **2004**, *4*, 527.
[23] C. J. Murphy, T. K. Sau, A. Gole, C. J. Orendorff, *MRS. Bull.* **2005**, *30*, 349.
[24] M. E. Stewart, C. R. Anderton, L. B. Thompson, J. Maria, S. K. Gray, J. A. Rogers, R. G. Nuzzo, *Chem. Rev.* **2008**, *108*, 494.
[25] B. Wiley, Y. Sun, J. Chen, H. Cang, Z.-Y. Li, X. Li, Y. Xia, *MRS. Bull.* **2005**, *30*, 356.
[26] J. Maria, T. T. Truong, J. Yao, T.-W. Lee, R. G. Nuzzo, S. Leyffer, S. K. Gray, J. A. Rogers, *J. Phys. Chem. C* **2009**, *113*, 10493.
[27] J. N. Anker, W. P. Hall, O. Lyandres, N. C. Shah, J. Zhao, R. P. V. Duyne, *Nat. Mater.* **2008**, *7*, 442.
[28] V. Malyarchuk, M. E. Stewart, R. G. Nuzzo, J. A. Rogers, *Appl. Phys. Lett.* **2007**, *90*, 203113/1.
[29] J. Yao, M. E. Stewart, J. Maria, T.-W. Lee, S. K. Gray, J. A. Rogers, R. G. Nuzzo, *Angew. Chem. Int. Ed.* **2008**, *47*, 5013.
[30] J. P. Camden, J. Dieringer, J. Zhao, R. P. Van Duyne, *Acc. Chem. Res* **2008**, *41*, 1653.
[31] R. Gordon, D. Sinton, K. L. Kavanagh, A. G. Brolo, *Acc. Chem. Res.* **2008**, *41*, 1049.
[32] D. A. Stuart, A. J. Haes, C. R. Yonzon, E. M. Hicks, R. P. Van Duyne, *IEE Proc.- Nanobiotechnol.* **2005**, *152*, 13.
[33] K. A. Willets, R. P. V. Duyne, *Annu Rev Phys Chem.* **2007**, *58*, 267.
[34] A. J. Baca, T. T. Truong, L. R. Cambrea, J. M. Montgomery, S. K. Gray, D. Abdula, T. R. Banks, J. Yao, R. G. Nuzzo, J. A. Rogers, *Appl. Phys. Lett.* **2009**, *94*, 243109.
[35] M. G. Albrecht, J. A. Creighton, *J. Am. Chem. Soc.* **1977**, *99*, 5215.
[36] M. Fleischmann, P. J. Hendra, A. J. McQuillan, *Chem. Phys. Lett.* **1974**, *26*, 163.
[37] D. L. Jeanmaire, R. P. Van Duyne, *Journal of Electroanalytical Chemistry* **1977**, *84*, 1.
[38] P. Johansson, H. Xu, M. Käll, *Phys. Rev. B* **2005**, *72*, 035427.
[39] K. Kneipp, Y. Wang, H. Kneipp, L. T. Perelman, I. Itzkan, R. R. Dasari, M. S. Feld, *Phys. Rev. Lett.* **1997**, *78*, 1667.
[40] A. M. Michaels, Jiang, L. Brus, *J. Phys. Chem. B* **2000**, *104*, 11965.
[41] S. Nie, S. R. Emory, *Science* **1997**, *275*, 1102.
[42] H. Xu, E. J. Bjerneld, M. Käll, L. Börjesson, *Phys. Rev. Lett.* **1999**, *83*, 4357.
[43] H. X. Xu, J. Aizpurua, M. Kall, P. Apell, *Phys. Rev. E* **2000**, *62*, 4318.
[44] C. L. Haynes, R. P. Van Duyne, *J. Phys. Chem. B* **2003**, *107*, 7426.
[45] A. Tao, F. Kim, C. Hess, J. Goldberger, R. He, Y. Sun, Y. Xia, P. Yang, *Nano Lett.* **2003**, *3*, 1229.
[46] Q. Yu, P. Guan, D. Qin, G. Golden, P. M. Wallace, *Nano Lett.* **2008**, *8*, 1923.
[47] J. T. Bahns, Q. Guo, J. M. Montgomery, S. K. Gray, H. M. Jaeger, L. Chen, *J. Phys. Chem. C* **2009**, *113*, 11190.
[48] J. J. Baumberg, T. A. Kelf, Y. Sugawara, S. Cintra, M. E. Abdelsalam, P. N. Bartlett, A. E. Russell, *Nano Lett.* **2005**, *5*, 2262.
[49] J. Grand, P.-M. Adam, A.-S. Grimault, A. Vial, M. L. de la Chapelle, J.-L. Bijeon, S. Kostcheev, P. Royer, *Plasmonics* **2006**, *1*, 135.
[50] W. Rechberger, A. Hohenau, A. Leitner, J. R. Krenn, B. Lamprecht, F. R. Aussenegg, *Opt. Commun.* **2003**, *220*, 137.
[51] C.-K. Chang, D.-Z. Lin, C.-S. Yeh, C.-K. Lee, Y.-C. Chang, M.-W. Lin, J.-T. Yeh, J.-M. Liu, *Appl. Phys. Lett.* **2007**, *90*, 061113/1.
[52] J. Dintinger, S. Klein, T. W. Ebbesen, *Adv. Mater.* **2006**, *18*, 1267.
[53] F. Przybilla, C. Genet, T. W. Ebbesen, *Appl. Phys. Lett.* **2006**, *89*, 121115.
[54] S. I. Bozhevolnyi, V. S. Volkov, E. Devaux, J.-Y. Laluet, T. W. Ebbesen, *Nature* **2006**, *440*, 508.
[55] X. Zhang, C. Yonzon, R. P. V. Duyne, *J. Mat. Res.* **2006**, *21*, 1083.
[56] X. Zhang, A. V. Whitney, J. Zhao, E. M. Hicks, R. P. V. Duyne, *J. Nanosci. Nanotechnol.* **2006**, *6*, 1920.
[57] C. L. Haynes, R. P. Van Duyne, *J. Phys. Chem. B* **2001**, *105*, 5599.
[58] P. Freunscht, R. P. Van Duyne, S. Schneider, *Chem. Phys. Lett.* **1997**, *281*, 372.
[59] S.-M. Yang, S. G. Jang, D.-G. Choi, S. Kim, H. K. Yu, *Small* **2006**, *2*, 458.
[60] J. Prikulis, P. Hanarp, L. Olofsson, D. Sutherland, M. Kaell, *Nano Lett.* **2004**, *4*, 1003.
[61] J. Henzie, M. H. Lee, T. W. Odom, *Nat. Nanotechnol.* **2007**, *2*, 549.
[62] E.-S. Kwak, J. Henzie, S.-H. Chang, S. K. Gray, G. C. Schatz, T. W. Odom, *Nano Lett.* **2005**, *5*, 1963.
[63] J. Henzie, J. Lee, M. H. Lee, W. Hasan, T. W. Odom, *Annu. Rev. Phys. Chem.* **2009**, *60*, 147.
[64] H. Gao, J. Henzie, T. W. Odom, *Nano Lett.* **2006**, *6*, 2104.
[65] J. Henzie, J. E. Barton, C. L. Stender, T. W. Odom, *Acc. Chem. Res* **2006**, *39*, 249.
[66] H. Gao, J. M. McMahon, M. H. Lee, J. Henzie, S. K. Gray, G. C. Schatz, T. W. Odom, *Opt. Express* **2009**, *17*, 2334.
[67] M. E. Stewart, M. J. Motala, J. Yao, L. B. Thompson, R. G. Nuzzo, *Proc. Inst. Mech. Eng. Part N: J. Nanoeng. Nanosyst.* **2007**, *220*, 81.
[68] V. Malyarchuk, F. Hua, N. H. Mack, V. T. Velasquez, J. O. White, R. G. Nuzzo, J. A. Rogers, *Opt Express* **2005**, *13*, 5669.
[69] V. N. Truskett, M. P. C. Watts, *Trends Biotechnol.* **2006**, *24*, 312.
[70] S.-H. Chang, S. K. Gray, G. C. Schatz, *Opt. Express* **2005**, *13*, 3150.
[71] A. Taflove, S. C. Hagness, *Computational Electrodynamics: The Finite-Difference Time-Domain*, Artech House, Boston **2005**.
[72] K. L. Shuford, M. A. Ratner, S. K. Gray, G. C. Schatz, *Appl. Phys. B* **2006**, *84*, 11.
[73] N. H. Mack, J. W. Wackerly, V. Malyarchuk, J. A. Rogers, J. S. Moore, R. G. Nuzzo, *Nano Lett.* **2007**, *7*, 733.

[74] T. T. Truong, J. Maria, J. Yao, M. E. Stewart, T.-W. Lee, S. K. Gray, R. G. Nuzzo, J. A. Rogers, *Nanotechnol.* **2009**, *20*, 434011.
[75] E. Delamarche, H. Schmid, B. Michel, H. Biebuyck, *Adv. Mater.* **1997**, *9*, 741.
[76] F. Hua, Y. Sun, A. Gaur, M. A. Meitl, L. Bilhaut, L. Rotkina, J. Wang, P. Geil, M. Shim, J. A. Rogers, *Nano Lett.* **2004**, *4*, 2467.
[77] T. W. Odom, J. C. Love, D. B. Wolfe, K. E. Paul, G. M. Whitesides, *Langmuir* **2002**, *18*, 5314.
[78] H. Schmid, B. Michel, *Macromolecules* **2000**, *33*, 3042.
[79] T. T. Truong, R. Lin, S. Jeon, H. H. Lee, J. Maria, A. Gaur, F. Hua, I. Meinel, J. A. Rogers, *Langmuir* **2007**, *23*, 2898.
[80] J. P. Rolland, R. M. Van Dam, D. A. Schorzman, S. R. Quake, J. M. DeSimone, *J. Am. Chem. Soc.* **2004**, *126*, 2322.
[81] G. D. Rothrock, B. Maynor, J. P. Rolland, J. M. DeSimone, *Proc. SPIE-Int. Soc. Opt. Eng.* **2006**, *6152*, 61523.
[82] J. P. Rolland, E. C. Hagberg, G. M. Denison, K. R. Cater, J. M. DeSimone, *Angew. Chem. Int. Ed.* **2004**, *43*, 5796.
[83] D. Barchiesi, D. Macías, L. Belmar-Letellier, D. van Labeke, M. Lamy de la Chapelle, T. Toury, E. Kremer, L. Moreau, T. Grosges, *Appl. Phys. B* **2008**, *93*, 177.
[84] X. J. Jiao, J. Goeckeritz, S. Blair, M. Oldham, *Plasmonics* **2009**, *4*, 37.
[85] B. A. Sexton, B. N. Feltis, T. J. Davis, *Sens. Actuators A* **2008**, *141*, 471.
[86] A. Dahlin, M. Zach, T. Rindzevicius, M. Kall, D. S. Sutherland, F. Hook, *J. Am. Chem. Soc.* **2005**, *127*, 5043.
[87] E. Hutter, J. H. Fendler, *Adv. Mater.* **2004**, *16*, 1685.
[88] A. D. McFarland, R. P. Van Duyne, *Nano Lett.* **2003**, *3*, 1057.
[89] T. Rindzevicius, Y. Alaverdyan, A. Dahlin, F. Hook, D. S. Sutherland, M. Kall, *Nano Lett.* **2005**, *5*, 2335.
[90] A. G. Brolo, R. Gordon, B. Leathem, K. L. Kavanagh, *Langmuir* **2004**, *20*, 4813.
[91] E. M. Hicks, X. Zhang, S. Zou, O. Lyandres, K. G. Spears, G. C. Schatz, R. P. Van Duyne, *J. Phys. Chem. B* **2005**, *109*, 22351.
[92] A. B. Dahlin, J. O. Tegenfeldt, F. Hook, *Anal. Chem.* **2006**, *78*, 4416.
[93] D. A. Stuart, A. J. Haes, C. R. Yonzon, E. M. Hicks, R. P. Van Duyne, *IEE Proc. Nanobiotechnol.* **2005**, *152*, 13.
[94] L. S. Jung, C. T. Campbell, T. M. Chinowsky, M. N. Mar, S. S. Yee, *Langmuir* **1998**, *14*, 5636.
[95] A. Kumar, H. A. Biebuyck, G. M. Whitesides, *Langmuir* **1994**, *10*, 1498.
[96] J. C. Love, L. A. Estroff, J. K. Kriebel, R. G. Nuzzo, G. M. Whitesides, *Chem. Rev.* **2005**, *105*, 1103.
[97] R. G. Nuzzo, D. L. Allara, *J. Am. Chem. Soc.* **1983**, *105*, 4481.
[98] R. G. Nuzzo, L. H. Dubois, D. L. Allara, *J. Am. Chem. Soc.* **1990**, *112*, 558.
[99] R. G. Nuzzo, F. A. Fusco, D. L. Allara, *J. Am. Chem. Soc.* **1987**, *109*, 2358.
[100] R. G. Nuzzo, B. R. Zegarski, L. H. Dubois, *J. Am. Chem. Soc.* **1987**, *109*, 733.
[101] B. Zhao, J. S. Moore, *Langmuir* **2001**, *17*, 4758.
[102] D. J. Beebe, J. S. Moore, Q. Yu, R. H. Liu, M. L. Kraft, B.-H. Jo, C. Devadoss, *Proc. Natl. Acad. Sci. U. S. A.* **2000**, *97*, 13488.
[103] D. J. Beebe, J. S. Moore, J. M. Bauer, Q. Yu, R. H. Liu, C. Devadoss, B.-H. Jo, *Nature* **2000**, *404*, 588.
[104] P. J. Flory, *Principles of Polymer Chemistry*, in: Cornell University Press, Ithica, NY **1953**.